

Comparative study of quantum Otto and Carnot engines powered by a spin working substance

M. Y. Abd-Rabbou ^{1,*}, Atta ur Rahman ², Mikhail A. Yurischev ³ and Saeed Haddadi ^{4,5,†}


¹Mathematics Department, Faculty of Science, Al-Azhar University, Nasr City 11884, Cairo, Egypt

²School of Physics, University of Chinese Academy of Science, Yuquan Road 19A, Beijing 100049, China

³Federal Research Center of Problems of Chemical Physics and Medicinal Chemistry, Russian Academy of Sciences, Chernogolovka 142432, Moscow Region, Russia

⁴Faculty of Physics, Semnan University, P.O. Box 35195-363, Semnan, Iran

⁵Saeed's Quantum Information Group, P.O. Box 19395-0560, Tehran, Iran

 (Received 8 April 2023; revised 18 June 2023; accepted 11 August 2023; published 7 September 2023)

Quantum Otto and Carnot engines have recently been receiving attention due to their ability to achieve high efficiencies and powers based on the laws of quantum mechanics. This paper discusses the theory, progress, and possible applications of quantum Otto and Carnot engines, such as energy production, cooling, and nanoscale technologies. In particular, we investigate a two-spin Heisenberg system that works as a substance in quantum Otto and Carnot cycles while exposed to an external magnetic field with both Dzyaloshinsky-Moriya and dipole-dipole interactions. The four stages of engine cycles are subject to analysis with respect to the heat exchanges that occur between the hot and cold reservoirs, alongside the work done during each stage. The operating conditions of the heat engine, refrigerator, thermal accelerator, and heater are all achieved. Moreover, our results demonstrate that the laws of thermodynamics are strictly upheld and the Carnot cycle produces more useful work than that of the Otto cycle.

DOI: [10.1103/PhysRevE.108.034106](https://doi.org/10.1103/PhysRevE.108.034106)

I. INTRODUCTION

The development of thermodynamics as a physical theory began with the aim of improving the efficiency of large-scale machinery, specifically steam engines [1,2]. Despite its origins in applications, thermodynamics has been very successful in developing universal principles, such as the second law. Quantum thermodynamics has emerged due to the rapid developments of quantum technologies, which has led to the expansion of the thermodynamics framework to include nonlocal systems [3]. One of the major objectives of quantum thermodynamics is to find the optimal use of quantum features for enhanced performance of quantum devices. Besides, in the recent quantum mechanical developing world, the connection between nonlocal systems and thermodynamics has become an active and exciting area of research [4,5].

Quantum heat engines (QHEs) are devices that generate power by harnessing the dynamics of heat between the hot and cold reservoirs, in accordance with the laws of thermodynamics and quantum mechanics [6]. Generally, the heat flow is typically carried out by a working substance, and the work output, efficiency, and power of a QHE depend on factors such as the temperature difference between the reservoirs, the type of working substance, and the cycle that the QHE operates [7]. QHEs can use a variety of quantum working entities to generate positive work, such as multilevel systems [8], coupled spins [9], harmonic oscillators [10], relativistic particles [11],

squeezed spin states [12], optomechanical systems [13], and others. QHEs exhibit exotic manifestations due to the nonlocal properties of the aforementioned working substances [13–16]. For example, a QHE can outperform a traditional Carnot heat engine in terms of performance and can retrieve work from a heat reservoir [17]. Therefore, QHEs have remained a subject of extensive research for efficient energy utilization and complementing their classical counterparts over the past decades.

From the point of view of the difference between a quantum and a classical heat engine, it is worth mentioning that the traditional thermodynamic analyses assume the existence of reservoir temperatures. It means that the reservoirs satisfy the Boltzmann distribution among their energy levels; however, many quantum systems are not Boltzmann-like. Thus, entropy flows can no longer be implied by the energy flows and corresponding temperatures. In particular, it is more accurate to analyze the energy and entropy flows independently. That is why a nonthermal quantum reservoir can turn some of its energy into work without the need for a second reservoir simply by using some of its information (“entropy deficiency”), a possibility that a classical thermal reservoir does not have. In other words, the key differences between quantum and classical heat engines lie in the nature of their working substances, such as the quantization of energy levels in quantum systems, the potential for quantum-enhanced efficiency, and the scale of their practical applications.

In 1959, Geusic *et al.* [18] introduced the concept of quantum thermal machines, quantum cycles, and quantum engines, where an analogy between the Carnot heat engine and three-level maser has been made to study the thermodynamic laws

*m.elmalky@azhar.edu.eg

†saeed@ssqig.com

at the quantum scale. To comprehend the quantum process, the same authors also proposed the concept of a quantum heat pump [19]. Also, various kinds of quantum thermal machines based on the Scovil principles have been suggested. For instance, a QHE based on an open quantum system has been proposed by Alicki [20] (see also Ref. [21]), and it has been further extended to derive a relation between the external driving force and estimated power by Kosloff [22]. The contribution of Kosloff with Geva led to the foundation of using multiple spin-1/2 systems as working substances in QHEs [23]. In Ref. [24] the authors extended this idea to quantum refrigerators using multiple spin-1/2 particles. The concept of a nonclassical three-cycle and a quantum amplifier based on a three-level system as a QHE has been devised [25] (see also [26]). Moreover, the notion of quantum Otto and Stirling cycles with swap heat engines has been established [27–29]. In the wake of these developments, a plethora of QHE devices that utilize ultracold atoms [30], quantum dots [31], Bose and Fermi gases [32], and trapped particles [33] have been the subject of extensive research.

Efficiency estimation is a common method in thermodynamics for comparing the work performance of heat engines [34]. Some analytical relationships for efficiency, work, power, and fluctuations have been obtained for a quantum Otto engine with a hot-squeezed and a cold thermal reservoir [35]. An optimal limit for increasing work and efficiency has been discovered for an Otto cycle utilizing long-range interactions [36]. The performance and efficiency of QHEs based on the Otto cycle have been studied using coupled and uncoupled spin models [37]. High power output and efficiency have been investigated for an endoreversible Otto cycle using quasispin systems of Cesium impurities [38]. An adiabatic deformation-based QHE has been observed to improve machine performance by increasing output work and efficiency while lowering work fluctuations [39]. In a recent study [40], the authors analyzed the efficiency of the Otto cycle in both classic and quantum versions. However, few studies have explored QHEs based on Heisenberg spin chains [41–43]. For example, the efficiency and valuable work of hybrid qubit-qutrit Heisenberg XXX, XXZ, and XYZ spin chains have been investigated [44]. The effects of coherence on efficiency and positive work have also been studied (see Refs. [45–47] and references quoted therein). In a magnetic Otto QHE, Kuznetsova *et al.* [48] evaluated the efficiency of QHEs for different choices of model parameters under Dzyaloshinsky-Moriya (DM) and Kaplan-Shehtman-EntinWohlman-Aharony (KSEA) interactions.

As QHEs are primarily regulated by temperature differences between the hot and cold reservoirs, Heisenberg spin chains are more optimal to be considered than the general spin-states. Motivated by this, we consider a two-qubit Heisenberg XYZ system influenced by DM interaction, external magnetic field, and dipole-dipole interaction working in both quantum Otto and quantum Carnot cycles. We aim to obtain useful work and improve performance by adjusting system parameters and identifying optimal conditions. Both the quantum Otto and quantum Carnot cycles are assumed in four stages, where the system undergoes modification and is then recycled.

A comparative study of the quantum Otto and Carnot cycles for spin systems would be beneficial for the following reasons. First, it would complement existing works that have mainly focused on the quantum Otto cycle, enhancing our understanding of the broader picture. Second, this study could reveal potential advantages or disadvantages of the Carnot cycle for spin systems. Such a comparison could identify universal features that apply to both cycles, as well as the differences that arise due to their distinct working mechanisms involving different thermodynamic processes. Our results could guide the design of more efficient spin-based QHEs by determining which cycle is better suited for a given practical application and physical system. Moreover, this comparative study would add to our fundamental understanding of thermodynamics in the quantum regime by exploring the similarities and differences between these two iconic thermodynamic cycles for a new class of physical systems, namely, spin systems.

This work is organized in the following order. In Sec. II we introduce a Hamiltonian used as a spin working substance and the modeling of quantum Otto and Carnot cycles. In Sec. III we discuss the main results obtained for the considered model. We express the significance, applications, and future experimental prospects of our work in Sec. IV. Finally, the conclusion and outlook are given in Sec. V.

II. SPIN-WORKING SUBSTANCE AND CONSIDERED CYCLES

Let us consider a working substance comprising a two-spin Heisenberg XYZ system influenced by DM and dipolar interactions and exposed to an external magnetic field. The mentioned Hamiltonian at an arbitrary distance vector \vec{r} can be written as [49–51]

$$\begin{aligned} \hat{H} = & J_x \hat{\sigma}_x^a \hat{\sigma}_x^b + J_y \hat{\sigma}_y^a \hat{\sigma}_y^b + J_z \hat{\sigma}_z^a \hat{\sigma}_z^b + M(\hat{\sigma}_z^a + \hat{\sigma}_z^b) \\ & + \vec{D} \cdot (\vec{\sigma}^a \times \vec{\sigma}^b) + \frac{\gamma}{|\vec{r}|^5} [|\vec{r}|^2 \vec{\sigma}^a \cdot \vec{\sigma}^b - 3(\vec{r} \cdot \vec{\sigma}^a)(\vec{r} \cdot \vec{\sigma}^b)], \end{aligned} \quad (1)$$

where $\vec{\sigma}^{a,b} = \{\hat{\sigma}_x, \hat{\sigma}_y, \hat{\sigma}_z\}^{a,b}$ are the Pauli spin operators associated with qubits a and b , J_i ($i = x, y, z$) is the coupling strength of two spins, M is the transverse magnetic field along z direction, $\vec{D} = \{D_x, D_y, D_z\}$ is the DM vector coupling, and γ denotes the dipolar interaction strength which is given by $\frac{\mu_0 \gamma_0^2}{16\pi}$ where μ_0 is the magnetic permeability of free space and γ_0 indicates the gyromagnetic constant. Finally, $\vec{r} = \{r_x, r_y, r_z\}$ is the distance vector with $\vec{r} = \vec{r}^b - \vec{r}^a$. For the sake of simplicity, the Hamiltonian model (1) can be reconstructed after expanding all terms as

$$\begin{aligned} \hat{H} = & R_x \hat{\sigma}_x^a \hat{\sigma}_x^b + R_y \hat{\sigma}_y^a \hat{\sigma}_y^b + R_z \hat{\sigma}_z^a \hat{\sigma}_z^b + M(\hat{\sigma}_z^a + \hat{\sigma}_z^b) \\ & + C_{x,yz}^+ \hat{\sigma}_x^a \hat{\sigma}_y^b + C_{x,yz}^- \hat{\sigma}_y^a \hat{\sigma}_x^b + C_{x,z,y}^- \hat{\sigma}_x^a \hat{\sigma}_z^b \\ & + C_{x,z,y}^+ \hat{\sigma}_z^a \hat{\sigma}_x^b + C_{y,z,x}^+ \hat{\sigma}_y^a \hat{\sigma}_z^b + C_{z,y,x}^- \hat{\sigma}_z^a \hat{\sigma}_y^b, \end{aligned} \quad (2)$$

where $R_i = J_i + \frac{\gamma}{|\vec{r}|^5} (|\vec{r}|^2 - 3r_i^2)$ and $C_{m,n,l}^\pm = \pm D_l - \frac{3\gamma}{|\vec{r}|^5} r_m r_n$. The density operator $\hat{\rho}$ of a typical system at thermal equilibrium can be written as $\hat{\rho} = \exp(-\beta \hat{H})/Z$, where $\beta = 1/k_B T$, while T and k_B are the temperature and Boltzmann

constant, respectively. Note that $Z = \text{Tr}[\exp(-\beta\hat{H})]$ is the partition function.

Now, the eigenvalues of the Hamiltonian (2) in the standard computational basis formed by $\mathcal{B} = \{|00\rangle, |01\rangle, |10\rangle, |11\rangle\}$ for z -directional spin-1/2 operator can be straightforwardly obtained as

$$E_{1,2} = \frac{1}{2}(x_1 \pm x_2^-), \quad E_{3,4} = -\frac{1}{2}(x_1 \mp x_2^+), \quad (3)$$

where

$$\begin{aligned} x_1 &= \sqrt{\frac{1}{3}\left(2a + L_1 + \frac{L_2}{L_1}\right)}, \\ x_2^\pm &= \sqrt{\frac{1}{3}\left(4a - L_1 - \frac{L_2}{L_1}\right)} \pm \frac{b}{x_1}, \\ L_1 &= \left(\frac{-2L_3 + \sqrt{4L_3^2 - 4L_2^3}}{2}\right)^{\frac{1}{3}}, \\ L_2 &= a^2 + 12c, \\ L_3 &= a^3 - 36ac + 54b^2, \end{aligned} \quad (4)$$

with

$$\begin{aligned} a &= 4M^2 + 2R_z^2 + 2|e_{12}|^2 + 2|e_{13}|^2 + |e_{14}|^2 + |e_{23}|^2, \\ b &= R_z(|e_{23}|^2 - |e_{14}|^2 - 4M^2) + 2\text{Re}[e_{12}e_{13}(e_{14} - e_{23})], \\ c &= R_z^4 + R_z^2(-4M^2 + 2|e_{12}|^2 + 2|e_{13}|^2 - |e_{14}|^2 - |e_{23}|^2) \\ &\quad + (|e_{12}|^2 - |e_{13}|^2)^2 + |e_{23}|^2(4M^2 + |e_{14}|^2) \\ &\quad + 2\text{Re}[2R_z e_{12}e_{13}(e_{14} + e_{23}) + e_{14}(e_{12}^2 e_{23} + e_{13}^2 e_{32})], \end{aligned} \quad (5)$$

$$e_{12} = C_{z,xy}^+ - iC_{y,z,x}^-, \quad e_{13} = C_{z,xy}^- - iC_{y,z,x}^+ = e_{31}^*,$$

$$e_{14} = R_x - R_y - i(C_{x,y,z}^+ + C_{x,y,z}^-) = e_{41}^*,$$

$$e_{23} = R_x + R_y - i(C_{x,y,z}^+ - C_{x,y,z}^-).$$

The corresponding occupation probabilities based on the structures of eigenenergy are given by

$$p_i = \frac{1}{Z} \exp\left(\frac{-E_i}{k_B T}\right), \quad (6)$$

where $Z = \sum_{i=1}^4 \exp\left(\frac{-E_i}{k_B T}\right)$, and $k_B = 1$ in this paper.

Thus, the occupation probabilities for our considered system in the standard basis \mathcal{B} are obtained as

$$\begin{aligned} p_1 &= \frac{1}{Z} e^{-\frac{x_1+x_2^-}{2T}}, \quad p_2 = \frac{1}{Z} e^{-\frac{x_1-x_2^-}{2T}}, \\ p_3 &= \frac{1}{Z} e^{\frac{x_1-x_2^+}{2T}}, \quad p_4 = \frac{1}{Z} e^{\frac{x_1+x_2^+}{2T}}, \end{aligned} \quad (7)$$

with

$$Z = e^{-\frac{x_1+x_2^-}{2T}} + e^{-\frac{x_1-x_2^-}{2T}} + e^{\frac{x_1-x_2^+}{2T}} + e^{\frac{x_1+x_2^+}{2T}}.$$

A. Modeling of quantum Otto cycle

The quantum simulation of the thermal Otto cycle comprises two quantum adiabatic and two quantum isochoric

processes. It is supposed the exchange coupling J_i and external magnetic field M remain unchanged throughout the four stages, while the DM and dipolar interaction strengths vary during the cycle. Notice that we will use the abbreviations “ h ” and “ c ” for “hot” and “cold” reservoirs, respectively, in all equations. The four stages of the quantum Otto cycle are described as follows:

Stage A \rightarrow B: This is an isochoric heating process, in which the working substance is coupled to a hot reservoir and is allowed to absorb an amount of heat slowly. The structures of eigenenergy E_i are conserved, while the occupation probabilities become changed p_i^h . In the meantime, the control parameters are $\bar{D} = \bar{D}^h$ and $\gamma = \gamma^h$, while no work is done.

Stage B \rightarrow C: The second stage of this cycle is the adiabatic part, where the eigenenergy levels are changed from E_i^h to E_i^c . This is done by decoupling the two-qubit system from the reservoirs (the process is quasistatic), thereby preventing heat transfer into or out of the system ($\Delta Q = 0$). The control parameters \bar{D}^h and γ^h are varied to \bar{D}^c and γ^c , respectively, such that $\bar{D}^c < \bar{D}^h$ and $\gamma^c < \gamma^h$.

Stage C \rightarrow D: The third part of the Otto cycle is the reverse process of $A \rightarrow B$, where the working substance is coupled to a cold reservoir, and heat is slowly removed from the two-qubit system to keep the temperature constant. Besides, the occupation probabilities are changed to p_i^c .

Stage D \rightarrow A: The final part of the Otto cycle is the reverse process of the second stage, in which the eigenenergy structures change to E_i^h and the control parameters are reverted to \bar{D}^h and γ^h . It is done by decoupling the system from the reservoirs, and the energy is returned to the system as work done.

The heat transfer processes from the hot thermal reservoir to the working substance and vice versa, during the absorption of heat (Q_{Ot}^h) and the emission of heat (Q_{Ot}^c), can be expressed as

$$Q_{Ot}^h = \text{Tr}[H^h \rho^h] - \text{Tr}[H^h \rho^c] = \sum_{i=1}^4 E_i^h (p_i^h - p_i^c) \quad (8)$$

and

$$Q_{Ot}^c = \text{Tr}[H^c \rho^c] - \text{Tr}[H^c \rho^h] = \sum_{i=1}^4 E_i^c (p_i^c - p_i^h). \quad (9)$$

According to the law of conservation of energy, the net work done by the Otto engine in the quantum adiabatic stages reads

$$\mathcal{W}_{Ot} = Q_{Ot}^h + Q_{Ot}^c. \quad (10)$$

As mentioned in Ref. [52], the four different operating modes can be observed for a quantum Otto engine, as shown in Table I.

B. Modeling of quantum Carnot cycle

In this subsection we present the quantum modeling of the classical Carnot cycle, which is carried out in four stages, to provide a reasonable comparison with the Otto heat engine. In this regard, the schematization of the Carnot cycle comprises two isothermal and two adiabatic processes. In the Carnot cycle the eigenenergy structures can change during a thermodynamic process. The two isothermal processes are $A \rightarrow B$

TABLE I. Operating modes of the quantum Otto engine depending on signs W_{Ot} , Q_{Ot}^h , and Q_{Ot}^c .

Mode	W_{Ot}	Q_{Ot}^h	Q_{Ot}^c
QHE	>0	>0	<0
Refrigerator	<0	<0	>0
Accelerator	<0	>0	<0
Heater	<0	<0	<0

and $C \rightarrow D$, in which the working substance is coupled to a hot and a cold heat reservoir at temperatures T^h and T^c , respectively. At each instant of these processes, the occupation probabilities are given by the Boltzmann distribution $p_i(n)$ with $n \in \{A, B, C, D\}$ and $i = 1, 2, 3, 4$. However, heat is transferred, and as a result, some work is done. Hence, the total entropy $S(n)$ increases and can be estimated using $S(n) = -k_B \sum_i p_i(n) \ln p_i(n)$. Besides, the two adiabatic processes are $B \rightarrow C$ and $D \rightarrow A$, where the eigenenergy structures are changed by the same ratio, i.e., $E_i(B) - E_j(B) = \frac{T^h}{T^c} \{E_i(C) - E_j(C)\}$ and $E_i(A) - E_j(A) = \frac{T^h}{T^c} \{E_i(D) - E_j(D)\}$ [53]. This condition is satisfied to ensure the equality of the final occupation populations, namely, $p_i(B) = p_i(C)$ and $p_i(A) = p_i(D)$. Moreover, the control parameters \vec{D} and γ are changed, while the total entropy $S(n)$ of the working substance remains invariant during this process.

By applying the heat exchange $dQ = TdS$ in the two quantum isothermal processes, the amount of absorbed heat from the heater Q_{Ca}^h and the amounts of heat released Q_{Ca}^c to the cold reservoir are defined, respectively, as [53,54]

$$Q_{\text{Ca}}^h = T^h \{S(B) - S(A)\}, \quad (11)$$

$$Q_{\text{Ca}}^c = T^c \{S(C) - S(D)\}. \quad (12)$$

From the first law of thermodynamics, one can express the work done by the quantum Carnot cycle as

$$W_{\text{Ca}} = Q_{\text{Ca}}^h + Q_{\text{Ca}}^c. \quad (13)$$

In classical thermodynamics, the efficiency of the Otto cycle is bounded by the Carnot efficiency [53–55]. In this study we explore the work done by the two quantum cycles and present a comparative analysis.

Notice, we have assumed here that the reservoirs are thermal. However, the optimal paths of the Otto and Carnot cycles may not proceed only through thermal states; e.g., the heat exchange mechanism can also be provided by the Lindblad formalism [56,57].

III. MAIN RESULTS AND DISCUSSION

In this section we discuss the performance of the quantum Otto and Carnot cycles at different distance vectors of the dipolar and DM interactions. The effects of these vectors on the work done, absorbed heat, and the amount of released heat are investigated. Besides, we assume equal final occupation populations in the adiabatic stages, such that $p_i(A) = p_i(D) = p_i^c$, and $p_i(B) = p_i(C) = p_i^h$ with $T^h = 2T^c = 2$. Without loss of generality, we also assume that the working substance is a ferromagnetic substance, initially with

$(J_x, J_y, J_z) = (-0.5, -1, -2)$. Moreover, the dipolar interaction in the adiabatic parts is altered by the same ratio as $\gamma^h = 2\gamma^c = 2\Gamma$ where Γ denotes the relative dipolar coupling. In addition, the distance vector \vec{r} and the DM interaction vector \vec{D} are set either along the x direction or z direction. The ability to analyze the system along both the x and z axes enables an examination of how the orientation of external influences impacts performance. Specifically, configuring the system such that the DM interaction and dipolar are orthogonal or parallel provides insight into which orientation leads to more optimal operation over the full cycle.

A. The Heisenberg model with x -directional dipolar interaction

Let us consider the case that the dipolar interaction is regulated along x axis with vector $\vec{r} = (1, 0, 0)$. However, the DM interaction is considered along (1) the x direction and (2) the z direction.

1. The case that the DM interaction is along the x direction

When the DM interaction is along the x direction, the explicit form of the DM coupling in the hot or cold reservoir may be written as $D_x^{h(c)}$. In this case, one can use the Hamiltonian (2) to obtain the occupation probabilities p_i^h and p_i^c .

In order to provide further explanation of the working substance in hot and cold reservoirs, we have plotted the occupation probabilities p_i^h and p_i^c in Fig. 1 as a function of relative dipolar coupling Γ . We assume that the distance vector and DM interaction in the x direction where $\vec{r} = (1, 0, 0)$ and $D_x^h = 2D_x^c = 2$ with the parameters $T^h = 2T^c = 2$, and $\gamma^h = 2\gamma^c = 2\Gamma$. In the absence of the magnetic field when $\Gamma < -1$, Figs. 1(a) and 1(b) show that the occupation probabilities $p_4^h = p_4^c = 1$ while the other probabilities $p_i^h = p_i^c = 0$ and $i = 1, 2$, and 3. In the meantime, quantum thermodynamic correlations must be equal to zero. In the context of the diamagnetic dipole (characterized by negative Γ values), no engines can meet the criteria outlined in Table I. If $\Gamma > 2$, one can see $p_4^h < p_4^c$ and $p_3^h > p_3^c$, where p_i^h are parallel in competition with the population p_i^c . In this region, and according to the first law of thermodynamics, these differences may generate one of the heat engines mentioned in Table I, and it depends on the amount of absorbed heat from the heater and the amounts of heat released to the cold reservoir. In the presence of a magnetic field with $M = 2$, Figs. 1(c) and 1(d) show that for $\Gamma < -1$, the working substance is only populated p_4^h and p_4^c , where $p_4^h = p_4^c = 1$. This situation leads to zero contribution of thermodynamic correlations. However, if $\Gamma > 2$, the populations p_4^h and p_4^c are rival to the populations p_3^h and p_3^c . As a result, this region displays either positive or negative quantum thermodynamic correlations, leading to one of the quantum engines.

To illustrate the quantum thermodynamic correlations, we have plotted Fig. 2, which displays the absorbed and released heat, as well as work done by the quantum Otto and Carnot cycles as a function of the relative dipolar coupling Γ with $D_x^h = 2D_x^c = 2$. Figure 2(a) shows that for $M = 0$, the work done by the quantum Carnot cycle is consistently greater than that of the Otto cycle. It is noticed that when $\Gamma > 3$, the Otto cycle's work done is zero, i.e., the energy exiting the system dissipates, while the work done by the Carnot

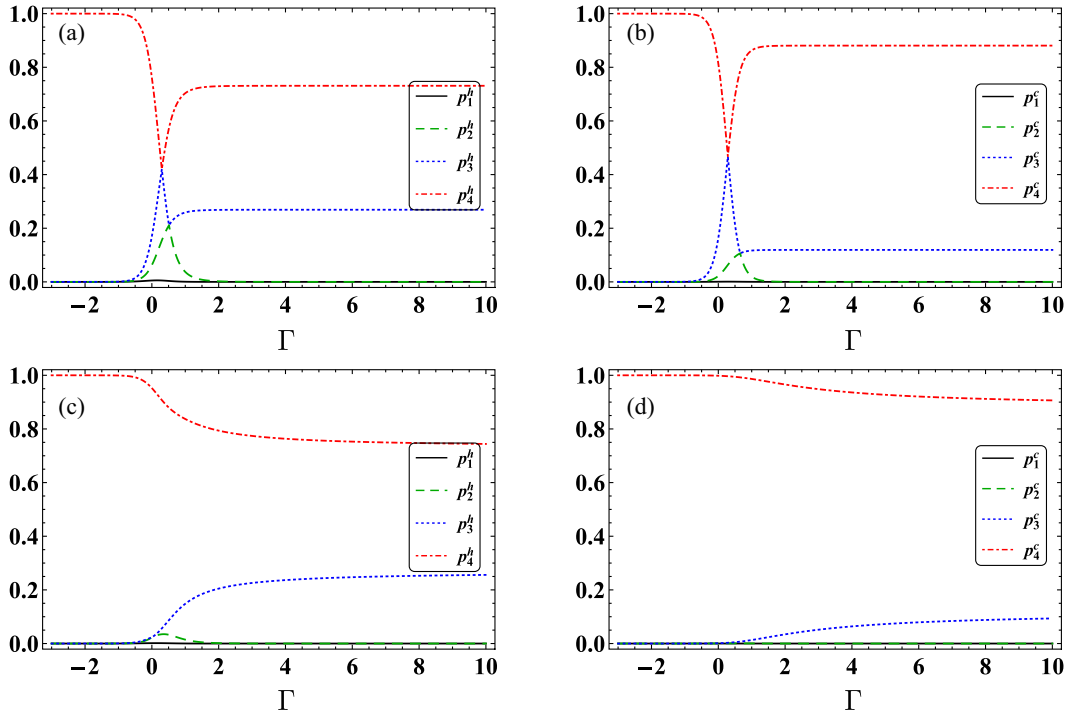


FIG. 1. Occupation probabilities against the relative dipolar coupling Γ , for the distance vector $\vec{r} = (1, 0, 0)$, with the parameters $T^h = 2T^c = 2$, $D_x^h = 2D_x^c = 2$, and $\gamma^h = 2\gamma^c = 2\Gamma$. (a) The occupation probabilities of the hot reservoir p_i^h with $M = 0$. (b) The occupation probabilities of the cold reservoir p_i^c with $M = 0$. Plots (c) and (d) are the same as plots (a) and (b), respectively, but for $M = 2$.

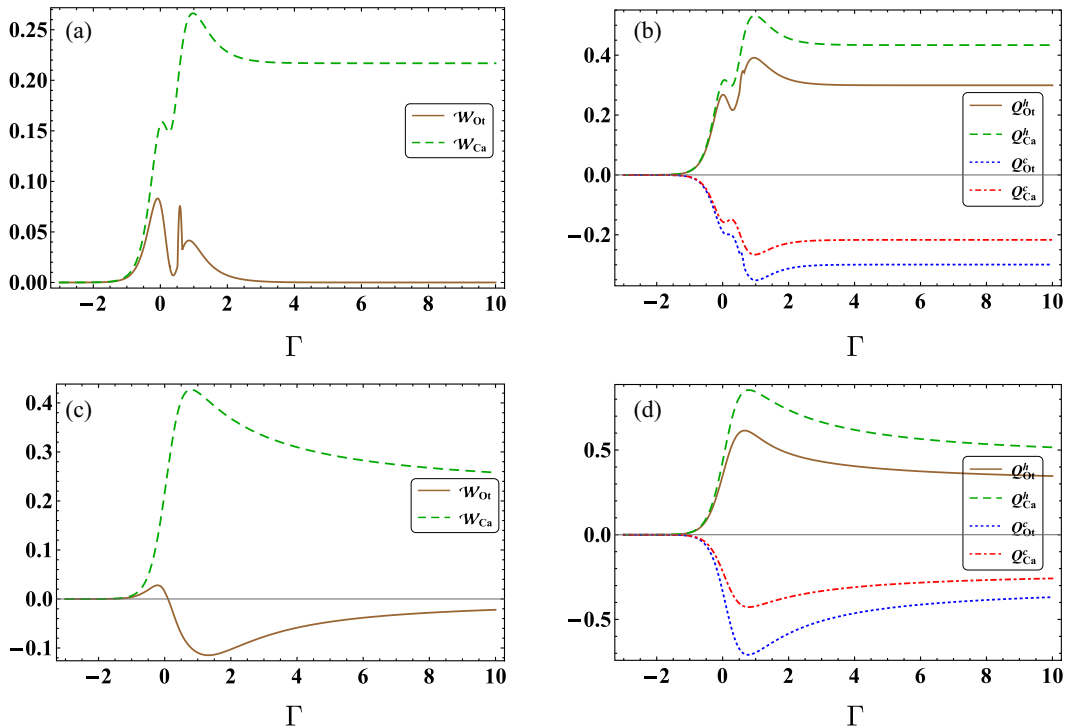


FIG. 2. Quantum thermodynamical quantities of the quantum Otto and Carnot cycles against the relative coupling Γ with the distance vector $\vec{r} = (1, 0, 0)$ and the parameters $2T^c = T^h = 2$, $D_x^h = 2D_x^c = 2$, $\gamma^h = 2\gamma^c = 2\Gamma$, and $M = 0$. (a) The work done \mathcal{W}_{Ot} (\mathcal{W}_{Ca}) of the Otto (Carnot) cycle. (b) The absorbed heat Q_{Ot}^h (Q_{Ca}^h) and the released heat Q_{Ot}^c (Q_{Ca}^c) of the Otto (Carnot) cycle. Plots (c) and (d) are the same as plots (a) and (b) but for $M = 2$.

cycle remains fixed at approximately $\mathcal{W}_{Ca} \simeq 0.22$. Note that within the range of $-1 < \Gamma < 3$, the difference between the work done by the Carnot and Otto cycles is maximal. In the forenamed range, the work done by the Carnot cycle suffers insignificant oscillations before reaching a maximum and then plateauing at a constant value. On the contrary, the Otto engine exhibits revivals within the aforementioned range, it initially increases, then the work done is reversed, and finally, it saturates at zero. The revivals in the work done by the Otto engine show the energy exchange between the system and its coupled reservoirs, which is ultimately either completely lost or utilized as work done. However, when $\Gamma < -1$, there is no work done in the two cycles. This is due to the identical occupation probabilities in the hot and cold reservoirs, namely, zero or one (see Fig. 1). As a result, there is an insufficient contribution to the work done.

Figure 2(b) displays the absorbed heat $Q_{Ot}^h(Q_{Ca}^h)$ and the released heat $Q_{Ot}^c(Q_{Ca}^c)$ of the Otto (Carnot) cycle. It is clear that $Q_{Ot,Ca}^h \geq 0$ and $Q_{Ot,Ca}^c \leq 0$. This means that both the Carnot and Otto cycles do positive work and operate the system as a QHE. From Figs. 2(a) and 2(b), it is easy to deduce that the system in this case behaves like a QHE for the parameter regime of $-2 < \Gamma < 2.5$, where $\mathcal{W}_{Ot} > 0$, $Q_{Ot}^h > 0$, and $Q_{Ot}^c < 0$. Besides, it is also noticeable that the plots for Q_{Ot}^h and Q_{Ot}^c are varying in opposite directions, implying heat exchange between the hot and cold reservoirs within the specified range. This implies that for a working QHE, the two reservoirs must be constantly exchanging heat, and as the heat stops, the system stops working; see, e.g., the Otto cycle for $\Gamma \leq -2$ and $\Gamma > 2$.

The effect of an increased external magnetic field strength, i.e., $M = 2$, on quantum thermodynamic quantities is displayed in Figs. 2(c) and 2(d). It is apparent that the quantum heat regime is dependent on the presence of the external magnetic field. The maximum bounds of work done by the quantum Carnot cycle increase with an increased external magnetic field, while the work done by the quantum Otto cycle decreases to negative values after $\Gamma > 0.1$. This is due to the increased disorder induced by the external magnetic field, and therefore, the system does an insignificant amount of work. The detrimental impact of the external magnetic field on the Carnot engine is also evident, as the slope of \mathcal{W}_{Ca} appears to decrease with Γ . The output value of \mathcal{W}_{Ot} in Fig. 2(c) shows that the working substance contributes to the negative work extraction in the positive dipole regime. Moreover, Fig. 2(d) indicates that the heat taken from or into the system by the two cycles coincides. In the case of the Otto or Carnot cycle, the heat released into the hot reservoir is negative for $\Gamma > -1$, while the heat absorbed by the system from the cold reservoir is positive for all values of Γ . Additionally, the slopes of Q_{Ot}^h and Q_{Ot}^c alter in opposite directions, and as the difference between the heat exchange of the hot and cold reservoirs becomes maximum, the negative work done by the Otto cycle also reaches maximum. Notice that the functions Q_{Ot}^h and Q_{Ot}^c show that the cycle takes some time to start working after the heat exchange. From Figs. 2(c) and 2(d), it can be deduced that the QHE action can be achieved for $-1 < \Gamma < 0.1$, where $\mathcal{W}_{Ot} > 0$, $Q_{Ot}^h > 0$, and $Q_{Ot}^c < 0$. However, this holds for only a brief period of time, and as Γ increases or decreases beyond this range, the work done becomes either zero or negative.

Therefore, realistic QHEs are restricted by certain bounds, which must be established in order to obtain a positive work performance.

Furthermore, we get a possible thermal accelerator [52], in which $\mathcal{W}_{Ot} \leq 0$, $Q_{Ot}^h \geq 0$, and $Q_{Ot}^c \leq 0$. Interestingly, the presence of an external magnetic field can increase the maximum bounds of work by the Carnot cycle and the minimum bounds of work done by the Otto cycle. Finally, we conclude that the positivity of the work by the quantum Otto engine can depend on the presence or absence of the external magnetic field. Regarding the Otto cycle, one can easily deduce that when the external magnetic field is absent, the work done is always greater than when the external magnetic field is nonzero.

2. The case that the DM interaction is along the z direction

Let us suppose that the position vector of the dipole-dipole interaction is oriented along the x direction, while the DM interaction is along the z direction.

According to this assumption, the occupation probabilities in the hot and cold reservoirs exhibit behavior analogous to that shown in Fig. 1, but with varying upper and lower bounds in p_4^h , p_3^h , p_4^c , and p_3^c . Hence, there is no need to plot them separately, since their impact will appear in the thermodynamic correlations.

Figure 3 presents a comparative analysis of thermodynamic correlations in quantum Otto and Carnot cycles, under the same conditions as in Fig. 2, but with the DM interaction directed along the z axis, such that $D_z^h = 2D_z^c = 2$. In Fig. 3(a) both cycles exhibit zero work done for $\Gamma < -1$, which increases with a rise in Γ , and the Otto and Carnot cycles start working positively. In comparison, the Carnot cycle starts working quicker than the Otto cycle, therefore, the fact remains consistent that no realistic engine can reach the efficiency of the Carnot heat engine. Besides, both cycles reach their maxima as Γ increases, with the Carnot cycle achieving a higher maximum. Eventually, the work done by the Otto cycle becomes negative as it enters a negative regime, with the negative work reaching a maximum value approximately at $\Gamma = 0$.

The work by the Carnot cycle lags that of the Otto cycle and enters the slight negative regimes while rising again into positive values and finally approaching a steady-state value for very large Γ . In comparison, the Otto cycle repeatedly oscillates in the nonpositive regimes and approaches a work output limit of zero for large Γ values. In Fig. 3(b) we plot the heat absorption and emission for both cycles. As can be seen, there is only one peak and valley evident. Specifically, the quantum Otto cycle involves negative values for the absorbed heat Q_{Ot}^h from the working substance reservoirs at $0.3 \lesssim \Gamma \lesssim 1$, while the released heat is always $Q_{Ot}^c \leq 0$. In the mentioned region, the engine tends to become a heater [52].

In Figs. 3(c) and 3(d), we depict the impact of an increased external magnetic field strength $M = 2$ with z -directed DM interaction on the work done, heat absorption, and emission in both the Otto and Carnot cycles. For $\Gamma < -2$, the work done in both cycles is zero, meaning that quantum engines based on Otto and Carnot cycles cannot operate in this parameter region. At $\Gamma = -1$, the Carnot and Otto cycles start approaching

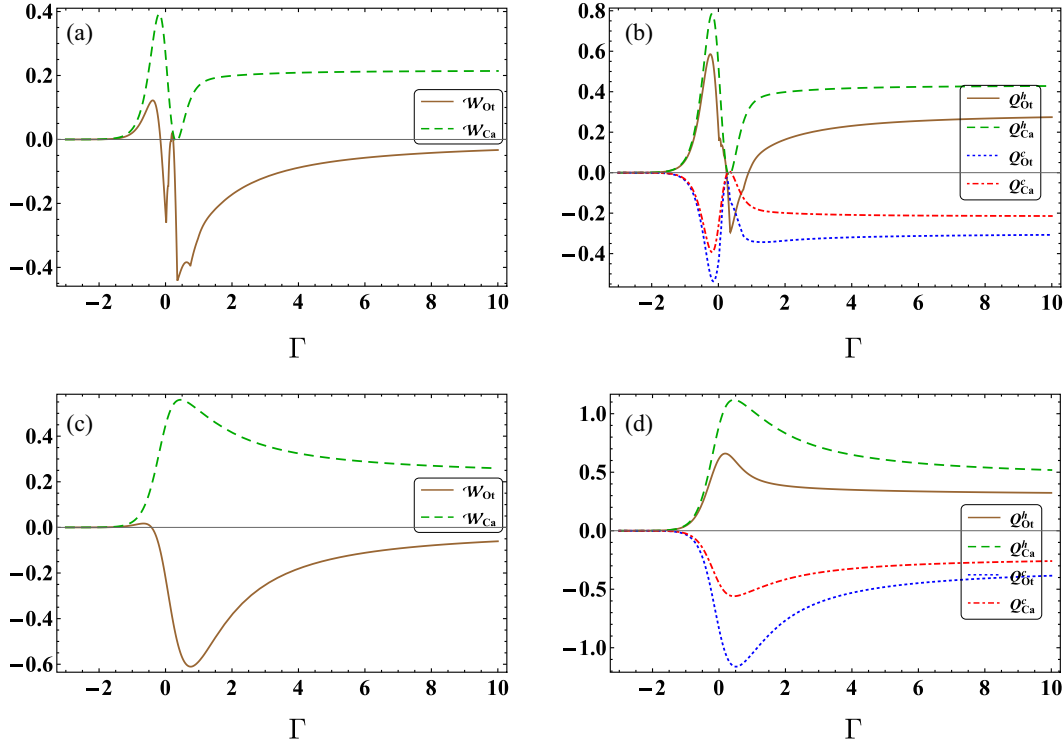


FIG. 3. Quantum thermodynamical quantifiers of the quantum Otto and Carnot cycles against the relative coupling Γ with the same parameters as Fig. 2, but for $D_z^h = 2D_z^c = 2$.

positive work, but the former has a significantly larger work output than the latter, which is negligible in the Otto cycle. As shown in Fig. 3(c), the work done in the Otto cycle rapidly reverses and enters the negative regime, i.e., $\mathcal{W}_{Ot} < 0$. As illustrated in Fig. 3(d), this matter is rooted in Eq. (10) with $Q_{Ot}^h \geq 0$ and $Q_{Ot}^c \leq 0$, representing a thermal accelerator [52]. A comparison of Figs. 3(b) and 3(d) reveals an interesting observation, i.e., a heater becomes a thermal accelerator in the presence of the magnetic field in the $0.3 \lesssim \Gamma \lesssim 1$ region.

In general, one can easily see that the maximum and minimum bounds of the work done by the Carnot and Otto cycles increase as the external magnetic field increases, respectively. Besides, in agreement with Fig. 3(a), the work done in the Otto cycle approaches zero because of the constant reduction in heat exchange between the hot and cold reservoirs. This observation is supported by Fig. 3(d), which shows a reduction in the negative output of work done with decreasing difference between Q_{Ot}^h and Q_{Ot}^c .

From Figs. 3(c) and 3(d), one can also depict that the Otto cycle behaves as a QHE at $\Gamma < -0.5$, where the heat absorbed and work done are positive, and the heat released is negative [52]. Nevertheless, when $\Gamma > -0.5$, one can get a possible thermal accelerator since the system may be absorbing heat from the working substance and releasing heat to the reservoir with negative work in the case of the Otto cycle.

It is important to note that the work done for the x -directed DM interaction explored in Fig. 2 differs from that when the DM interaction strength is oriented along the z direction. Hence, not only the magnetic field but also the direction of the DM interaction can affect the output performance of the

two cycles. Compared to the x -directed DM interaction case, the work done with the z -directed DM interaction seems less positive and highly negative in the Otto cycle. On the contrary, the work done in the Carnot cycle with $M = 0$ or 2 and the z -directed DM interaction achieves a higher maximum than that obtained with the x -directed DM interaction. Thus, the Otto cycle is more negatively affected than the Carnot cycle by the z -directed DM interaction. Notice, the work done for the Otto cycle suffers a transition from the positive regime to the negative one, while the work done in the Carnot engine alters between the relative minimum and maximum in the positive regime. Thereby, the Carnot cycle in the given conditions is working as a QHE. In agreement with the ideal assumption, \mathcal{W}_{Ca} always remains greater than \mathcal{W}_{Ot} .

B. The Heisenberg model with z -directional dipolar interaction

In this subsection, we assume that the dipolar interaction is set along the z direction with unit vector $\vec{r} = (0, 0, 1)$. However, the DM interaction is set along the x direction and z direction.

1. The case that the DM interaction is along the x direction

Assuming that the DM interaction is oriented along the x direction and the position vector of dipole-dipole interaction along the z direction, the Hamiltonian (2) can be used to derive the thermodynamic correlations.

Figure 4 illustrates the quantum thermodynamic quantities for the two cycles with the distance vector of dipole-dipole interaction aligned along the z direction, while the parameters remain unchanged from those presented in Fig. 2. At the onset,

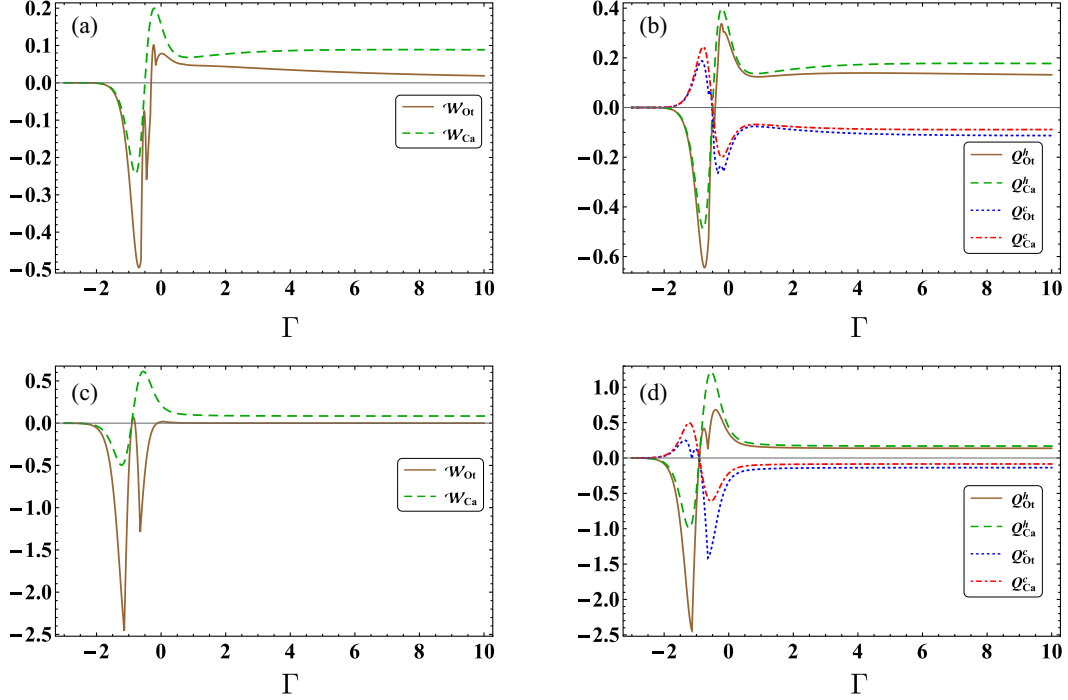


FIG. 4. Quantum thermodynamical quantities of the quantum Otto and Carnot cycles against the relative coupling Γ with the distance vector $\vec{r} = (0, 0, 1)$ and the parameters $T^h = 2T^c = 2$, $D_x^h = 2D_x^c = 2$, $\gamma^h = 2\gamma^c = 2\Gamma$, and $M = 0$. (a) The work done \mathcal{W}_{Ot} (\mathcal{W}_{Ca}) of the Otto (Carnot) cycle. (b) The absorbed heat Q_{Ot}^h (Q_{Ca}^h) and released heat Q_{Ot}^c (Q_{Ca}^c) of the Otto (Carnot) cycle. Plots (c) and (d) are the same as plots (a) and (b) but for $M = 2$.

when $\Gamma < -2$ in Fig. 4(a), the work done for both cycles remains zero. As $\Gamma \rightarrow -0.5$, the work done during both the Otto and Carnot cycle reaches negative minima. Therefore, one can see that the work done is also controlled by the direction of the distance vector \vec{r} , and the results obtained are different from those given in Figs. 2 and 3. From the relative negative minima, the slopes of the work done approach positive regimes and achieve higher maxima. Notably, the negative work done in the Otto cycle exhibits a faster dynamical speed compared to that observed in the Carnot cycle. Conversely, the slopes of the work done approach maxima in the positive regimes and reveal that the Carnot cycles are more proficient and active in sensing heat absorption and converting it to QHE compared to the Otto cycles. Finally, the slopes decrease slightly and achieve final saturation levels, indicating that no further work is performed. Besides, in Fig. 4(b) the absorbed and released heat is initially zero. However, within the region $-2 < \Gamma < -0.5$, heat flows from the system towards the considered reservoir, transforming the quantum Otto engine into a refrigerator where $Q_{Ot}^c > -Q_{Ot}^h > 0$ and $\mathcal{W}_{Ot} < 0$ [52], although the system rapidly absorbs heat and the work done becomes positive. For $\Gamma > 2$, the heat transfer between the reservoirs stabilizes, and the considered working substance contributes to positive work in both the Otto and Carnot cycles.

On the other hand, according to Figs. 4(c) and 4(d), the external magnetic field induces negative work by both the Otto and Carnot cycles. It is notable that the minima of the negative work regions in both cycles are deeper than that detected for $M = 0$ in Fig. 4(a). However, soon the heat exchange and the quantum refrigeration process become reversed, and

the working substance starts to gain heat. In the region of $-1 \lesssim \Gamma \lesssim -0.5$, the positive work done in the Carnot cycle achieves the maximum. Unlike this, in the Otto cycle, we have almost negative work done in the mentioned interval. Soon the quantum refrigeration condition is violated, and the zero-work limit is reached because of no further heat exchange between the working substance and heat reservoirs. Note that the positive work done by the Carnot cycle when $M = 2$ is much greater than that observed in the case when $M = 0$. Therefore, a stronger external magnetic field may support the Carnot cycles when considering the x -directed DM interaction with $\vec{r} = (0, 0, 1)$. For comparison, the differences between these results and those presented in Fig. 2 can be followed.

2. The case that the DM interaction is along the z direction

Finally, we prepare the DM interaction in the z direction and consider $r_z = 1$. In this case we have plotted Fig. 5 to demonstrate the thermodynamics correlation.

Figures 5(a) and 5(b) show the thermodynamics of the work done and heat exchanges between the hot and cold reservoirs for the Otto and Carnot cycles with the zero external magnetic field $M = 0$ and the DM interaction strength given by $D_z^h = 2D_z^c = 2$. Initially, for $\Gamma < -2$, the work done in both the Otto and Carnot cycles is zero for all the considered cases. In the range of $-1.5 \lesssim \Gamma \lesssim -0.5$, the Otto and Carnot cycles perform negative work, as shown in Fig. 5(a), and achieve relative minima. This means that the heat released (Q_{Ot}^c) exceeds the heat absorbed (Q_{Ot}^h), which is also visible in Fig. 5(b). In the mentioned region, the engine tends to become a refrigerator [52]. However, for $\Gamma > -0.5$, the

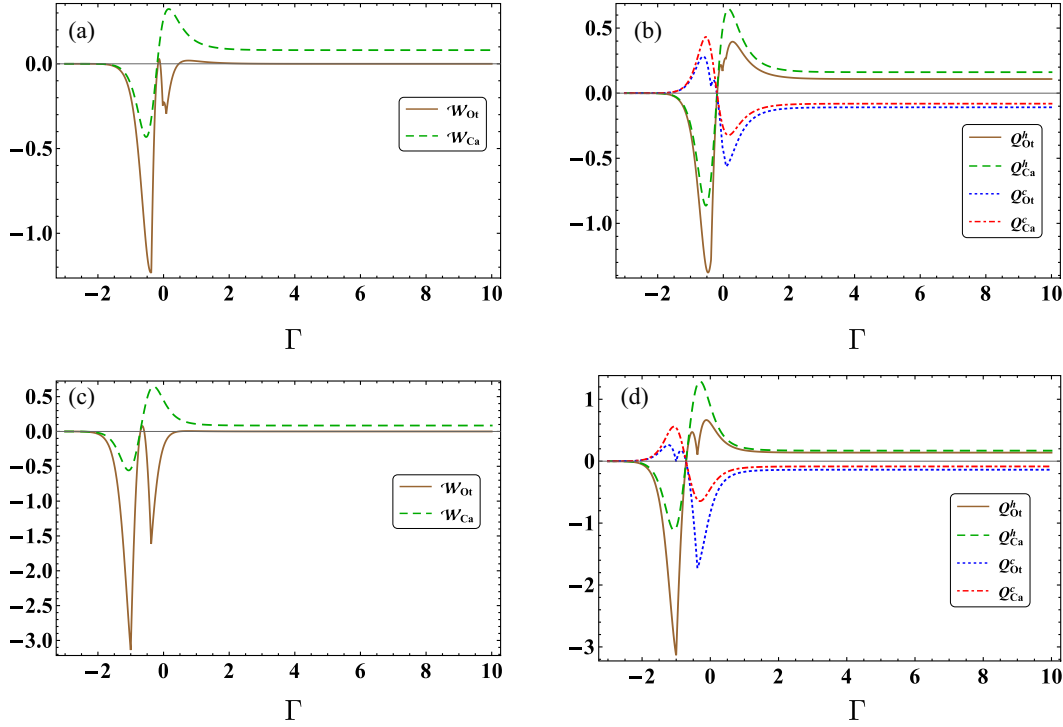


FIG. 5. Quantum thermodynamical quantifiers of the quantum Otto and Carnot cycles against the relative coupling Γ with the same parameters as Fig. 4, but for $D_z^h = 2D_z^c = 2$.

direction of heat exchange is reversed [see Fig. 5(b)], and the system absorbs heat. Therefore, the work done in the Otto cycle enters positive regimes, leaving the quantum refrigeration process. In the range of $0.5 \lesssim \Gamma \lesssim 1.5$, the Otto cycle does an insignificant amount of positive work and then saturates at the zero value. In comparison, the fact remains the same that $\mathcal{W}_{Ca} \geq \mathcal{W}_{Ot}$. Note that, for $\Gamma > 2$, there is no heat exchange between the working substance and the reservoirs. Therefore, the cycles further do not operate the QHE.

In Figs. 5(c) and 5(d), the impact of increased magnetic field strength on the thermodynamic quantities of work done and heat exchanges between the reservoirs for the Otto and Carnot cycles with $M = 2$, and the z -directed dipole-dipole interaction is investigated. Both cycles perform negative work done in the region of $-2 < \Gamma \lesssim -0.5$, which almost agrees with Fig. 5(a), but negative minima in Fig. 5(c) are deeper than those displayed in Fig. 5(a). This means that a stronger external magnetic field along the z -directional dipole-dipole interaction strongly supports the Otto and Carnot cycles to remain in the quantum refrigeration regime. For example, the work done in the mentioned range demonstrates this support. Nevertheless, when the heat exchange vanishes, the Otto cycle attains the zero-work limit. Note that there is a critical point such as in the range $-1 < \Gamma < -0.7$, where the Otto cycle enters the positive work done regimes and works as a QHE but is very insignificant. In the range $-1 \lesssim \Gamma \lesssim -0.5$, the Carnot cycle acts as a QHE and does maximal work at $\Gamma \approx 0.5$. With a further increase in Γ , the heat exchange settles down, as shown in Fig. 5(d), and both cycles no longer do any work. Notice, the higher strength of the external magnetic field with the z -directional dipolar interaction promotes quantum refrigeration. For example, see the behavior of the Otto cycle in

Figs. 5(a) and 5(c). This is because the heat released into the Otto engine becomes large for the increased strength of the external magnetic field; see, e.g., Figs. 5(b) and 5(d).

C. Analysis of the quantum Otto and Carnot cycles in different situations

In this subsection we present a comparison of the performance of quantum Otto and Carnot cycles implemented in different situations [58]. We primarily provide a comparative analysis of the positive and negative regimes for both cycles based on the heat exchange mechanism into or out of the working substance and heat reservoirs.

First, we focused on evaluating the influence of DM interaction in the x and z directions on the work done and heat exchanged in Otto and Carnot cycles. In this case we considered the position vector of the dipole-dipole interaction along the x direction. In the x -directed DM interaction, the Carnot cycle remains highly acting as a QHE. On the other hand, the Otto cycle acts as a QHE when a weak external magnetic is considered. When a strong external magnetic is applied, the engine tends to become a QHE only at a specific region of Γ , as seen in Fig. 2. In the z -directed DM interaction, the stronger external magnetic field enhances the positive work done by the Carnot cycle, but causes the Otto cycle to release heat and attain negative work, which is intriguing.

Second, the scenario completely changes from that witnessed in Figs. 2 and 3 when the z -directional dipole-dipole interaction is considered. For example, the Otto cycle achieves positive work done when the DM interaction is applied along the x direction, and in certain regions, the heat released by the Otto engine exceeded the heat absorption, hence, the engine

acts as a refrigerator. Meanwhile, the Carnot cycle exhibits both positive and negative work done regimes. However, the associated efficiency remains different from that witnessed against the x -directional dipole-dipole interaction. Moreover, when the z -directional dipole-dipole interaction is added, the Carnot cycle's work performance with respect to x -directional DM interaction is enhanced by increasing the external magnetic field. However, the opposite occurs when z -directional DM interaction is considered. In the case of the Otto cycle, the working substance with the z -directional DM interaction releases more heat than that with the x -directional DM interaction, therefore enhancing the negative work done limit. In terms of the relative dipole-dipole coupling Γ , there is always a finite interval in which both cycles either release or absorb heat. For all $\Gamma < -2$, no work is done by the cycles. However, as $\Gamma \rightarrow 0$, the cycles start working, going in either positive or negative regimes. Therefore, the range $-2 < \Gamma < 2$ always remains critical for many work done types in both Otto and Carnot cycles.

The current results for the Carnot and Otto cycles can be traced back to the positive and negative work obtained in the Stirling cycle, though with different parameters of the XX exchange interaction [59]. Recently, the authors of Ref. [60] studied the work done using two- and three-coupled spin-half Heisenberg XXX chain models to improve the efficiency of the quantum Otto thermal machines, where both the QHE and refrigeration regimes are studied against different ranges of magnetic field and KSEA interaction. To perform a detailed analysis, the thermodynamic terms such as work done and heat exchanges in Refs. [48,60] can be compared to those witnessed in our work. Using a Heisenberg XYZ model with both the DM anisotropic antisymmetric interaction and external magnetic field for a quantum Otto cycle, Ahadpour and Mirmasoudi [61] derived the transformation between the quantum heating and refrigeration process. In comparison, we find that the work done under certain conditions in the current study surpasses that derived by the authors in Ref. [61]. Similarly, compared to Ref. [62], in spin-1/2 systems influenced by the DM interaction driven by a changing magnetic field, the work done remains either positive or negative, and therefore agrees qualitatively with our results. Notably, Çakmak *et al.* [63] and then Altintas [64] investigated a working substance of two coupled qubits described by the Lipkin-Meshkov-Glick or Heisenberg XXX model in quantum Otto and Carnot engine cycles, and found positive work done in all situations.

IV. SIGNIFICANCE, APPLICATIONS, AND FUTURE EXPERIMENTAL PROSPECTS

The significance of quantum Otto and Carnot engines powered by a spin working substance lies in their potential to revolutionize the field of thermodynamics. Traditional engines, such as those used in cars and power plants, rely on the transfer of heat between two reservoirs to generate work. However, these engines are limited by the laws of thermodynamics, which dictate that there is a maximum efficiency that can be achieved. The spin-based systems as working substances allow us to manipulate them, which can lead to the creation of engines with higher operational efficiencies than the traditional ones. The quantum Otto and

Carnot engines are two examples of such engines that have been proposed and studied. The development of these engines has implications for a wide range of fields, including energy production, transportation, and computing. They could lead to more efficient and sustainable energy sources, as well as faster and more powerful computers. Thereby, the significance of these engines powered by a spin working substance lies in their potential to transform the way we think about energy and work, and to open up new possibilities for technological innovation.

One potential application of these engines is in the field of renewable energy. The quantum Otto and Carnot engines can be used to efficiently convert renewable energy sources such as solar, wind, and hydro into usable electricity. These engines can also be used to store excess energy generated from renewable sources for later use. Another potential application of these engines is in the field of quantum computing. The quantum Otto and Carnot engines can be used to power quantum computers, which are expected to be much faster and more powerful than classical computers. In addition, these engines can be used as cooling agents in the case of quantum computers to avoid thermal noises and associated losses for the proper functioning of computing-related protocols. These engines can be used to power spacecraft, allowing them to travel further and faster than current spacecraft. They can also be employed to generate electricity for spacecraft, which can reduce the reliance on solar panels. In the medical field, these engines can be used to power medical devices and implants. They can provide a reliable and efficient source of power for devices such as pacemakers and insulin pumps.

The experimental prospects of quantum Otto and Carnot engines powered by a spin working substance are exciting [65]. Researchers are currently working on developing and testing prototypes of these engines in the laboratory. One potential avenue for experimentation is the use of quantum dots as the spin working substance. These tiny semiconductor particles can be manipulated to create a spin current, which can then be used to power an engine. Researchers are also exploring the use of other quantum systems, such as trapped ions, superconducting qubits, and nitrogen-vacancy centres in diamonds [66–68]. Another area of research is the optimization of the engine design to maximize efficiency. This involves exploring different engine configurations, as well as developing new methods for controlling and manipulating the spin working substance.

V. CONCLUSION AND OUTLOOK

We have investigated a two-spin Heisenberg XYZ system influenced by both DM and dipole-dipole interactions as a working substance for the quantum Otto and Carnot cycles. In particular, we analysed the useful work and performance situations in different parameter choices, such as the external magnetic field, the coupling of DM interaction, and dipole-dipole interaction (along x or z directions). The quantum Otto and Carnot cycles were operated in four stages, where the system parameters undergo modification and are then repeated. The simultaneous study of the Otto and Carnot cycles allowed us to identify the resourcefulness of the considered schemes using the two-spin Heisenberg system. In light of our analysis,

we have demonstrated that the work output of the Otto cycle for the working substance under consideration is lower than that of the Carnot cycle. This observation is in accordance with the principles of classical thermodynamics. The reason for this lies in the fact that the Carnot cycle is an ideal cycle wherein all the added heat is efficiently converted into work, whereas the Otto cycle is a realistic cycle wherein a certain fraction of the added heat may be lost.

In general, the work done in both the Otto and Carnot cycles was found to be highly dependent on the strength of the external magnetic field and the direction of the DM and dipole-dipole interactions. In the absence of the external magnetic field, positive work can be produced using Otto and Carnot cycles when the DM and dipole interactions are set along the x direction. On the other hand, when the distance vector is set along the x direction and the DM interaction along the z direction, the work done by the Otto cycle and some portion of the Carnot cycle becomes negative. In the presence of an external magnetic field, the amount of work done has changed significantly compared to the case when there is no external magnetic field.

On the other hand, the work done by both cycles oscillates between negative and positive values when the distance vector is along the z axis, making the transition between working as a QHE, refrigerator, thermal accelerator, and heater. The Carnot engine cycle remains highly effective for QHE and less significant in the case of quantum refrigeration. In comparison, the Otto engine cycle under the current configuration can be easily driven to induce a refrigerator. Despite this, the Otto cycle can also be employed as QHE, accelerator, and heater under certain circumstances.

From the point of view of physical interpretation of our results, it can be briefly mentioned that both DM and dipolar interactions impact the energy levels, transition probabilities, spin canting, and anisotropic behavior of the spin system, all of which are crucial factors in the performance of these quantum engines. On one hand, the dipolar interactions can cause energy level splittings within the spin system. This can lead to modifications in the energy spectrum and alter

the population of spin states during the engine's operation, affecting the amount of work that can be extracted during the expansion and compression steps of the engine cycle. Dipolar interactions can also contribute to decoherence in the spin system. It can reduce the efficiency of the engine by limiting the ability to maintain quantum superpositions and manipulate quantum states. On the other hand, DM interactions can cause noncollinear arrangements of neighboring spins, leading to spin canting. This noncollinearity can impact the system's response to external magnetic fields during the engine cycle. Moreover, DM interactions introduce anisotropy in the spin system. This anisotropy affects the magnetic susceptibility and spin dynamics during the engine cycle, influencing the thermodynamic performance of the engine.

The outlook of quantum Otto and Carnot engines is promising [65]. These engines can potentially convert a larger portion of the input energy into useful work, using the principles of quantum entanglement and coherence. Currently, the development of quantum engines is in its early stages, and many technical challenges need to be overcome before practical applications can be realized. Research is ongoing to optimize the performance of quantum Otto and Carnot engines, and there is a growing interest in their applications in energy harvesting, refrigeration, and power conversion. With further advancements, quantum engines could revolutionize the way we generate and use energy.

No data sets were generated or analyzed during the current study.

ACKNOWLEDGMENTS

We are very grateful to Prof. Ming-Liang Hu for his valuable comments on the draft of this work. We also express our sincere gratitude to the esteemed referees for their helpful contribution in providing insightful and constructive comments. M.A.Y. was supported in part by a state task, the state registration number of the Russian Federation is AAAA-A19-119071190017-7. The authors declare that they have no known competing financial interests.

-
- [1] D. S. Cardwell and R. L. Hills, Thermodynamics and practical engineering in the nineteenth century, *The Development of Science and Technology in Nineteenth-Century Britain* (Routledge, London, 2017), p. 344.
 - [2] R. Alicki and R. Kosloff, Introduction to quantum thermodynamics: History and prospects, in *Thermodynamics in the Quantum Regime*, Fundamental Theories of Physics, Vol. 195, edited by F. Binder, L. Correa, C. Gogolin, J. Anders, and G. Adesso (Springer, Cham, 2018), pp. 1–33.
 - [3] P. Strasberg, G. Schaller, T. Brandes, and M. Esposito, Quantum and Information Thermodynamics: A Unifying Framework Based on Repeated Interactions, *Phys. Rev. X* **7**, 021003 (2017).
 - [4] R. Kosloff, Quantum thermodynamics: A dynamical viewpoint, *Entropy* **15**, 2100 (2013).
 - [5] K. Brandner and U. Seifert, Periodic thermodynamics of open quantum systems, *Phys. Rev. E* **93**, 062134 (2016).
 - [6] H. E. D. Scovil and E. O. Schulz-DuBois, Three-Level Masers as Heat Engines, *Phys. Rev. Lett.* **2**, 262 (1959).
 - [7] A. Insinga, B. Andresen, P. Salamon, and R. Kosloff, Quantum heat engines: Limit cycles and exceptional points, *Phys. Rev. E* **97**, 062153 (2018).
 - [8] H. T. Quan, P. Zhang, and C. P. Sun, Quantum heat engine with multilevel quantum systems, *Phys. Rev. E* **72**, 056110 (2005).
 - [9] B. Lin and J. Chen, Performance analysis of a quantum heat-pump using spin systems as the working substance, *Appl. Energy* **78**, 75 (2004).
 - [10] B. Lin and J. Chen, General performance characteristics of a quantum heat pump cycle using harmonic oscillators as the working substance, *Phys. Scr.* **71**, 12 (2005).

- [11] P. Chattopadhyay and G. Paul, Relativistic quantum heat engine from uncertainty relation standpoint, *Sci. Rep.* **9**, 16967 (2019).
- [12] F. Altintas, A. Ü. C. Hardal, and Ö. E. Müstecaplıoğlu, Quantum correlated heat engine with spin squeezing, *Phys. Rev. E* **90**, 032102 (2014).
- [13] K. Zhang and W. Zhang, Quantum optomechanical straight-twin engine, *Phys. Rev. A* **95**, 053870 (2017).
- [14] A. Friedenberger, Detecting quantum signatures in heat engines, Doctoral dissertation, Friedrich-Alexander-Universität Erlangen-Nürnberg (FAU, 2019).
- [15] J. Z. He, X. He, and J. Zheng, Entangled quantum heat engine based on two-qubit Heisenberg XY model, *Chinese Phys. B* **21**, 050303 (2012).
- [16] N. M. Myers and S. Deffner, Thermodynamics of statistical anyons, *PRX Quantum* **2**, 040312 (2021).
- [17] T. Denzler and E. Lutz, Efficiency fluctuations of a quantum heat engine, *Phys. Rev. Res.* **2**, 032062(R) (2020).
- [18] J. E. Geusic, E. O. Schulz-Du Bois, R. W. De Grasse, and H. E. D. Scovil, Three level spin refrigeration and maser action at 1500 mc/sec, *J. Appl. Phys.* **30**, 1113 (1959).
- [19] J. E. Geusic, E. O. Schulz-DuBios, and H. E. D. Scovil, Quantum equivalent of the Carnot cycle, *Phys. Rev.* **156**, 343 (1967).
- [20] R. Alicki, The quantum open system as a model of the heat engine, *J. Phys. A: Math. Gen.* **12**, L103 (1979).
- [21] B. Ahmadi, S. Salimi, and A. S. Khorashad, On the contribution of work or heat in exchanged energy via interaction in open bipartite quantum systems, *Sci. Rep.* **13**, 160 (2023).
- [22] R. Kosloff, A quantum mechanical open system as a model of a heat engine, *J. Chem. Phys.* **80**, 1625 (1984).
- [23] E. Geva and R. Kosloff, A quantum-mechanical heat engine operating in finite time. A model consisting of spin-1/2 systems as the working fluid, *J. Chem. Phys.* **96**, 3054 (1992).
- [24] J. He, J. Chen, and B. Hua, Quantum refrigeration cycles using spin-1/2 systems as the working substance, *Phys. Rev. E* **65**, 036145 (2002).
- [25] R. Kosloff and A. Levy, Quantum heat engines and refrigerators: Continuous devices, *Annu. Rev. Phys. Chem.* **65**, 365 (2014).
- [26] N. Gupt, S. Bhattacharyya, and A. Ghosh, Statistical generalization of regenerative bosonic and fermionic Stirling cycles, *Phys. Rev. E* **104**, 054130 (2021).
- [27] O. Abah, J. Rossnagel, G. Jacob, S. Deffner, F. Schmidt-Kaler, K. Singer, and E. Lutz, Single-Ion Heat Engine at Maximum Power, *Phys. Rev. Lett.* **109**, 203006 (2012).
- [28] Y. Yin, L. Chen, and F. Wu, Optimal power and efficiency of quantum Stirling heat engines, *Eur. Phys. J. Plus* **132**, 45 (2017).
- [29] R. Uzdin and R. Kosloff, The multilevel four-stroke swap engine and its environment, *New J. Phys.* **16**, 095003 (2014).
- [30] G. Barontini and M. Paternostro, Ultra-cold single-atom quantum heat engines, *New J. Phys.* **21**, 063019 (2019).
- [31] B. Sothmann, R. Sánchez, and A. N. Jordan, Thermoelectric energy harvesting with quantum dots, *Nanotechnology* **26**, 032001 (2015).
- [32] S. Sur and A. Ghosh, Quantum advantage of thermal machines with Bose and Fermi gases, *Entropy* **25**, 372 (2023).
- [33] S. An, J. N. Zhang, M. Um, D. Lv, Y. Lu, J. Zhang, Z. Q. Yin, H. T. Quan, and K. Kim, Experimental test of the quantum Jarzynski equality with a trapped-ion system, *Nat. Phys.* **11**, 193 (2015).
- [34] A. Ghosh, W. Niedenzu, V. Mukherjee, and G. Kurizki, Thermodynamic principles and implementations of quantum machines, in *Thermodynamics in the Quantum Regime*, Fundamental Theories of Physics, Vol. 195, edited by F. Binder, L. Correa, C. Gogolin, J. Anders, and G. Adesso (Springer, Cham, 2018), pp. 37–66.
- [35] J. Wang, J. He, and Y. Ma, Finite-time performance of a quantum heat engine with a squeezed thermal bath, *Phys. Rev. E* **100**, 052126 (2019).
- [36] Q. Wang, Performance of quantum heat engines under the influence of long-range interactions, *Phys. Rev. E* **102**, 012138 (2020).
- [37] R. S. Johal and V. Mehta, Quantum heat engines with complex working media, complete Otto cycles and heuristics, *Entropy* **23**, 1149 (2021).
- [38] Q. Bouton, J. Nettersheim, S. Burgardt, D. Adam, E. Lutz, and A. Widera, A quantum heat engine driven by atomic collisions, *Nature Commun.* **12**, 2063 (2021).
- [39] Y. Xiao, K. Li, J. He, and J. Wang, Performance of quantum heat engines enhanced by adiabatic deformation of trapping potential, *Entropy* **25**, 484 (2023).
- [40] F. J. Peña, O. Negrete, N. Cortés, and P. Vargas, Otto engine: Classical and quantum approach, *Entropy* **22**, 755 (2020).
- [41] G. F. Zhang, Entangled quantum heat engines based on two two-spin systems with Dzyaloshinski-Moriya anisotropic antisymmetric interaction, *Eur. Phys. J. D* **49**, 123 (2008).
- [42] F. Altintas and Ö. E. Müstecaplıoğlu, General formalism of local thermodynamics with an example: Quantum Otto engine with a spin-1/2 coupled to an arbitrary spin, *Phys. Rev. E* **92**, 022142 (2015).
- [43] H. P. Peng, M. F. Fang, and C. Y. Zhang, Quantum heat engine based on working substance of two particles Heisenberg XXX model with the Dzyaloshinskii-Moriya interaction, *Int. J. Theor. Phys.* **58**, 1651 (2019).
- [44] Y. Khelifi, A. El Allati, A. Salah, and Y. Hassouni, Quantum heat engine based on spin isotropic Heisenberg models with Dzyaloshinskii-Moriya interaction, *Int. J. Mod. Phys. B* **34**, 2050212 (2020).
- [45] H. P. Peng, M. F. Fang, M. Yu, and H. M. Zou, The influences of quantum coherence on the positive work and the efficiency of quantum heat engine with working substance of two-qubit Heisenberg XXX model, *Int. J. Theor. Phys.* **57**, 1872 (2018).
- [46] Y. H. Shi, H. L. Shi, X. H. Wang, M. L. Hu, S. Y. Liu, W. L. Yang, and H. Fan, Quantum coherence in a quantum heat engine, *J. Phys. A: Math. Theor.* **53**, 085301 (2020).
- [47] M. Asadian, S. Ahadpour, and F. Mirmasoudi, Quantum correlated heat engine in XY chain with Dzyaloshinskii-Moriya interactions, *Sci. Rep.* **12**, 7081 (2022).
- [48] E. I. Kuznetsova, M. A. Yurischev, and S. Haddadi, Quantum Otto heat engines on XYZ spin working medium with DM and KSEA interactions: Operating modes and efficiency at maximal work output, *Quantum Inf. Process.* **22**, 192 (2023).
- [49] H. Y. Kwon, K. M. Bu, Y. Z. Wu, and C. Won, Effect of anisotropy and dipole interaction on long-range order magnetic structures generated by Dzyaloshinskii-Moriya interaction, *J. Magn. Magn. Mater.* **324**, 2171 (2012).
- [50] Z. Liu, O. Ciftja, and H. Ian, Interplay of Dzyaloshinsky-Moriya and dipole-dipole interactions and their joint effects upon vortical structures on nanodisks, *Physica E* **90**, 13 (2017).

- [51] M. Y. Abd-Rabbou and E. M. Khalil, Dense coding and quantum memory assisted entropic uncertainty relations in a two-qubit state influenced by dipole and symmetric cross interactions, *Ann. Phys. (Berlin)* **534**, 2200204 (2022).
- [52] A. Solfanelli, M. Falsetti, and M. Campisi, Nonadiabatic single-qubit quantum Otto engine, *Phys. Rev. B* **101**, 054513 (2020).
- [53] H. T. Quan, Y. X. Liu, C. P. Sun, and F. Nori, Quantum thermodynamic cycles and quantum heat engines, *Phys. Rev. E* **76**, 031105 (2007).
- [54] H. T. Quan, Maximum efficiency of ideal heat engines based on a small system: Correction to the Carnot efficiency at the nanoscale, *Phys. Rev. E* **89**, 062134 (2014).
- [55] H. T. Quan, Quantum thermodynamic cycles and quantum heat engines. II, *Phys. Rev. E* **79**, 041129 (2009).
- [56] T. Feldmann, E. Geva, R. Kosloff, and P. Salamon, Heat engines in finite time governed by master equations, *Am. J. Phys.* **64**, 485 (1996).
- [57] A. Insinga, B. Andresen, and P. Salamon, Thermodynamical analysis of a quantum heat engine based on harmonic oscillators, *Phys. Rev. E* **94**, 012119 (2016).
- [58] T. Feldmann and J. P. Palao, Performance of quantum thermodynamic cycles, in *Thermodynamics in the Quantum Regime*, Fundamental Theories of Physics, Vol. 195, edited by F. Binder, L. Correa, C. Gogolin, J. Anders, and G. Adesso (Springer, Cham, 2018), pp. 67–85.
- [59] C. Purkait and A. Biswas, Performance of Heisenberg-coupled spins as quantum Stirling heat machine near quantum critical point, *Phys. Lett. A* **442**, 128180 (2022).
- [60] A. E. Makouri, A. Slaoui, and M. Daoud, Enhancing the performance of coupled quantum Otto thermal machines without entanglement and quantum correlations, *J. Phys. B: At. Mol. Opt. Phys.* **56**, 085501 (2023).
- [61] S. Ahadpour and F. Mirmasoudi, Coupled two-qubit engine and refrigerator in Heisenberg model, *Quantum Inf. Process.* **20**, 63 (2021).
- [62] L. M. Zhao and G. F. Zhang, Entangled quantum Otto heat engines based on two-spin systems with the Dzyaloshinski–Moriya interaction, *Quantum Inf. Process.* **16**, 216 (2017).
- [63] S. Çakmak, D. Türkpençe, and F. Altintas, Special coupled quantum Otto and Carnot cycles, *Eur. Phys. J. Plus* **132**, 554 (2017).
- [64] F. Altintas, Comparison of the coupled quantum Carnot and Otto cycles, *Physica A* **523**, 40 (2019).
- [65] A. Levy and D. Gelbwaser-Klimovsky, Quantum features and signatures of quantum thermal machines, in *Thermodynamics in the Quantum Regime*, Fundamental Theories of Physics, Vol. 195, edited by F. Binder, L. Correa, C. Gogolin, J. Anders, and G. Adesso (Springer, Cham, 2018), pp. 87–126.
- [66] S. T. Dawkins, O. Abah, K. Singer, and S. Deffner, Single atom heat engine in a tapered ion trap, in *Thermodynamics in the Quantum Regime*, Fundamental Theories of Physics, Vol. 195, edited by F. Binder, L. Correa, C. Gogolin, J. Anders, and G. Adesso (Springer, Cham, 2018), pp. 887–896.
- [67] N. Cottet and B. Huard, Maxwell’s demon in superconducting circuits, in *Thermodynamics in the Quantum Regime*, Fundamental Theories of Physics, Vol. 195, edited by F. Binder, L. Correa, C. Gogolin, J. Anders, and G. Adesso (Springer, Cham, 2018), pp. 959–981.
- [68] J. Klatzow, J. N. Becker, P. M. Ledingham, C. Weinzetl, K. T. Kaczmarek, D. J. Saunders, J. Nunn, I. A. Walmsley, R. Uzdin, and E. Poem, Experimental Demonstration of Quantum Effects in the Operation of Microscopic Heat Engines, *Phys. Rev. Lett.* **122**, 110601 (2019).